Supporting Information

Electrophoretic Fabrication of Alcohol-Stable $CsPbBr_3$ Nanocrystalline Photoelectrodes for Formaldehyde Production

Andrés F. Gualdrón-Reyes,[1,2,] Camilo A. Mesa,[1,]* Seul-Yi Lee,[1,3] Roser Fernández-Climent,[1,4] Sofia Masi,[1] Federica Aiello,[5] Federica Balzano,[6] Gloria Uccello-Barretta,[6] Ignacio Utreras-Asenjo,[2] Jeevan Torres,[1] Samiksha Mukesh Jain,[1] Carina Pareja-Rivera,[1] Hyo Joong Lee,[3] Jhonatan Rodríguez-Pereira,[7,8] Sixto Giménez[1,]* and Iván Mora-Seró[1,]**

[1]Institute of Advanced Materials (INAM), Universitat Jaume I (UJI), Avenida de Vicent Sos Baynat, s/n, 12071 Castelló de la Plana, Castellón, Spain.
[2]Facultad de Ciencias, Instituto de Ciencias Químicas, Isla Teja, Universidad Austral de Chile, 5090000, Valdivia, Chile.
[3]Department of Chemistry and Research Institute of Physics & Chemistry, Jeonbuk National University, Jeonju 561-756, South Korea.
[4]Department of Surface and Plasma Science, Faculty of Mathematics and Physics, Charles University, 180 00, Prague 8, Czech Republic.
[5]National Research Council, Institute for Chemical and Physical Processes (CNR-IPCF), Via G. Moruzzi, 1, 56124, Pisa, Italy.
[6]Department of Chemistry and Industrial Chemistry, University of Pisa, via G. Moruzzi 13, Pisa 56124, Italy.
[7]Center of Materials and Nanotechnologies, Faculty of Chemical Technology, University of Pardubice, Nam. Cs. Legii 565, 53002 Pardubice, Czech Republic.
[8]Central European Institute of Technology, Brno University of Technology, Purkyňova 123, 61200 Brno, Czech Republic.

Corresponding authors: andres.gualdron@uach.cl, camilo.mesa@icn2.cat, sjulia@uji.es, sero@uji.es.

1. Experimental section

1.1. Synthesis of $CsPbX_3$ (X = Br, I) perovskite nanocrystals (PNCs)

$CsPbX_3$ PNCs were synthesized with some modifications by a hot-injection method using Cs-oleate and PbX_2 solutions in stoichiometric amounts. First, Cs-oleate solution was prepared by mixing 0.407 g Cs_2CO_3 (202126, 99.9 %, Sigma-Aldrich), 1.4 mL oleic acid (OA, 364525, 90 %, Sigma–Aldrich) and 20 mL of 1-octadecene (1-ODE, O806, 90 %, Sigma-Aldrich) into a 50 mL three–neck flask, under vigorous stirring at vacuum conditions for 30 min at 80 ºC. Then, the temperature increased to 120 ºC and was kept under vacuum for 30 min. The mixture was heated at 150 °C under N_2 atmosphere, and the resultant transparent solution was later kept at 120 °C for further use. In another compartment, 0.9 g $PbBr_2$ (ABCR; AB202085, 99.998%) (1.0 g PbI_2 (ABCR; AB111058, 99.999%)) were mixed with 50 mL 1-ODE into a separate 100 mL three-neck flask and heated at 120 °C under vigorous stirring under vacuum conditions for 1 h. Then, a preheated mixture of 5.0 mL of each OA and oleylamine (HT OA100, 98 %, Sigma-Aldrich) was added to the reaction flask to favor the PbX_2 dissolution. The temperature of PbX_2 mixture was rapidly raised up to

170–180 °C, injecting 4 mL of preheated Cs-oleate swiftly. After the injection, green and red precipitates were obtained for $CsPbBr_3$ and $CsPbI_3$ in the colloidal solution, respectively. The reaction flask was quickly immersed into an ice bath for 5 s to quench the reaction. A two-step washing procedure was carried out for the isolation process. First, PNCs were centrifuged at 5000 RPM. for 5 min with methyl acetate (MeOAc, 296996, 99.5%, Sigma–Aldrich) (30 mL of PNCs liquor washed with 60 mL MeOAc). PNC's pellets were extracted from supernatant, redispersed with 5 mL of hexane (CHROMASOLV, 34859, 99.7 %, Honeywell), and mixed with 10 mL of MeOAc. The PNCs dispersion was centrifuged again at 5000 RPM for 5 min, removing the supernatant, and the final product was dissolved again in hexane at a concentration of ~60 $mg \cdot mL^{-1}$ (100 mM). Then, PNCs colloidal solutions in hexane were added into 1-butanol (1-BuOH, ACS reagent, ≥99.4%, Sigma-Aldrich, named hereafter as PNCs-BuOH dispersions) in different PNCs:BuOH volume ratio (1:7, 1:3, and 1:1) in absence and presence of diverse concentrations of didodecyldimethylammonium bromide (DDAB, 359025, 98%, Sigma Aldrich): 4.3, 8.5, 17, 43 and 85 mM.

1.2. Electrophoretic deposition of $CsPbX_3$ PNCs on FTO/TiO_2 electrodes

Fluorine-doped tin oxide (FTO) substrates (Pilkington, TEC-15) were rinsed with soap solution, Mili-Q water, acetone (211007.0716, 99.5 %, Panreac), and ethanol (141085.0716, 96 %, Panreac), each one for 15 min. After that, the substrates were dried with compressed air and cleaned under UV-O_3 for 15 min. Then, TiO_2 pastes (18NR-T, DYESOL, 30NR-D, Greatcell Solar) were coated on the substrates by Doctor blade method and annealed at 80 °C for 1 h, followed by 450 °C for 1 h. Here, the effect of TiO_2 layer on the PEC activity of the fabricated photoelectrode was evaluated by depositing 1, 2, and 3 mesoporous TiO_2 layers. Then, a two-electrode cell was assembled, where a FTO substrate (positive terminal) and the TiO_2/FTO electrode (negative terminal) were connected to a DC supply and immersed in the $CsPbX_3$ PNCs dispersed in BuOH. The voltage applied was 250 V during different electrophoretic deposition (ED) times (15, 30, and 60 s). After conducting the ED process, DDAB ligand was not removed since the presence of this ligand avoids the full permeation of a high density of alcohol molecules to reach the perovskite core, acting as a protective layer.

2. Characterization of morphology, structure, optical properties, and surface environment of the $CsPbX_3$ PNCs dispersions and films

The morphology of PNCs was studied through high-resolution transmission electron microscopy (HRTEM) using a field emission tunneling electron microscope (FE-TEM, Hitachi HF-3300, with applied bias of 300 kV. Then, Scanning Electron microscopy (SEM) measurements were carried out on PNCs films by using a JSM7001F microscope. The average particle size of PNCs was obtained from the TEM images using ImageJ software. The crystalline structure of PNCs films was analyzed by obtaining the corresponding X-ray

diffraction (XRD) profiles. A D4 Endeavor diffractometer from Bruker-AXS was used, using a Cu Kα radiation source (λ = 1.54056 Å) with the following factors: 2θ range of 5°-80° (0.02 °/step and 1.2 s/step). UV-vis spectra of films were acquired by using a UV-vis absorption spectrophotometer (Varian, Cary 300), in a wavelength range between 400–850 nm, while steady-state and time-resolved photoluminescence (PL) measurements were conducted through a photoluminescence spectrophotometer (Fluorolog 3-11, Horiba). An excitation wavelength of 420 nm was used to perform the steady state PL. Time-resolved PL measurements were performed at 405 nm pulsed laser (NanoLED-405L, <100 ps of pulse width, 1 MHz frequency). The absolute photoluminescence quantum yield (PLQY) films and corresponding PL spectra of PNCs were acquired through a Hamamatsu Absolute PLQY Measurement System C9920-02, equipped with an integrating sphere, at an excitation wavelength of 400 nm. Surface chemical composition and electronic state of PNCs were determined by X-ray Photoelectron Spectroscopy (XPS, ESCA-2SR, Scienta-Omicron). Spectra were recorded using monochromatic Al Kα = 1486.6 eV. The following sequence of spectra were recorded: survey spectra, C 1s, Pb 4f, Br 3d, O 1s, N 1s and C 1s again to verify the stability of the charge as the function of time. The survey and high-resolution spectra were recorded at a pass energy of 150 and 20 eV, respectively. The binding energy scale was referenced to adventitious carbon (284.8 eV). CasaXPS processing software (Casa Software Ltd) was used to analyze the data, and the quantitative analysis was made using sensitivity factors provided by the manufacturer. Then, NMR measurements were carried out on a Varian INOVA600 spectrometer equipped with a 5 mm probe operating at 600 MHz for ^{1}H nuclei; the temperature was controlled to ± 0.1°C. The proton spectra were acquired with the minimum spectral width required. The analyses in butanol-d_{10}/toluene-d_8 (2:1 v/v) mixture were carried out by using 8 s of relaxation delay, a 90° pulse of 12.4 μs, 32 scans and a gain of 2. The FID was acquired into 64 K data points during a 2.883 s acquisition time, and data were processed with 1.0 Hz line broadening. Deuterated solvents (toluene-d_8, butanol-d_{10}) were purchased from Deutero GmbH (Kastellaun, Germany).

3. Photoelectrochemical characterization of $CsPbX_3$ PNCs-based photoelectrodes

Chopped-light voltammetry, electrochemical impedance spectroscopy (EIS) and chronoamperometry (CA) measurements were performed in a three-electrode quartz cell, using an Autolab Potentiostat/Galvanostat. A nonaqueous Ag/Ag^+ electrode (filled with 0.01 M $AgNO_3$ and 0.1 M TBAP in acetonitrile) and a platinum wire were used as reference and counter electrode, respectively, while the PNCs photoelectrodes, showing a FTO/TiO_2/$CsPbBr_3$ architecture, were used as working electrodes. The supporting electrolyte was prepared dissolving 45 mM methylammonium bromide (MeBr, ≥99.99%, MS301000, Greatcell Solar), in different full alcohol environments: MeOH (CHROMASOLV, 34885, 99.9 %, Honeywell), EtOH (Absolute, ≥99.8% 20821.321, VWR Chemicals), 1-PrOH (ACS reagent, ≥99.5%, Sigma-Aldrich) and 1-BuOH (ACS reagent, ≥99.4%, Sigma-Aldrich) and solution based on MeOH:H_2O volume ratio = 1:1.

Photoelectrodes were backside illuminated with an Xe lamp (Oriel 300W) at standard 1 sun (100 mW·cm^{-2}), filtering the UV light with a 400 nm high-pass neutral filter to avoid the (photo)electrocatalytic activity of both TiO_2 layers. For linear sweep voltammetry curves, the scan rate was 10 mV·s^{-1}. For EIS, a frequency range of 100 kHz – 0.1 Hz was employed, applying a bias potential of 0.1 V *vs.* Ag/Ag$^+$. For CA, only 45 mM MeBr in MeOH solution was used for evaluating formaldehyde (CH_2O) production from MeOH oxidation, Faradic efficiency (FE) of the above conversion was calculated by Faraday's law: $FE = \frac{[\,]_{experimental}}{[\,]_{theoretical}} x\ 100$, where $[\,]_{theoretical}$ is the CH_2O concentration obtained by photoelectrolysis, calculated by estimating first the total generated CH_2O mol (η) using Faraday´s law: $\eta_{theoretical} = \frac{Q}{n.F}$, being Q is the accumulated charge recorded during CA (C), n is the number of electrons transferred in the reaction (n = 2), and F is the Faraday constant, 96485.33 C·mol^{-1}, and dividing by total electrolyte solution volume (25 mL). This concentration (in M) was converted into ppm. Then, $[\,]_{experimental}$ was determined through UV-Vis spectroscopy, by obtaining the corresponding UV-Vis spectra of samples composed by three separate aliquots (10 mL each one) extracted from the electrolytic solution [at t = 0 (blank), and t = 1800 s under visible light in absence (photolysis) and presence of photoanode] and mixed with 10 mL of 1M NaOH and 0.1 g of 4-amino-5-hydrazino-1,2,4-triazole-3-thiol and diluted to 25 mL in water, according with the procedure reported elsewhere.[1] Then, the generated formaldehyde was quantified using a calibration curve; see **Figure S13**. Lastly, in order to evaluate the long-term stability of the optimized $CsPbBr_3$ photoanode (8.5 Mm DDAB), CA profile was obtained by applying a bias potential of 0.1 V *vs.* Ag/Ag$^+$ for 1 h in 45 mM MeBr in MeOH solution.

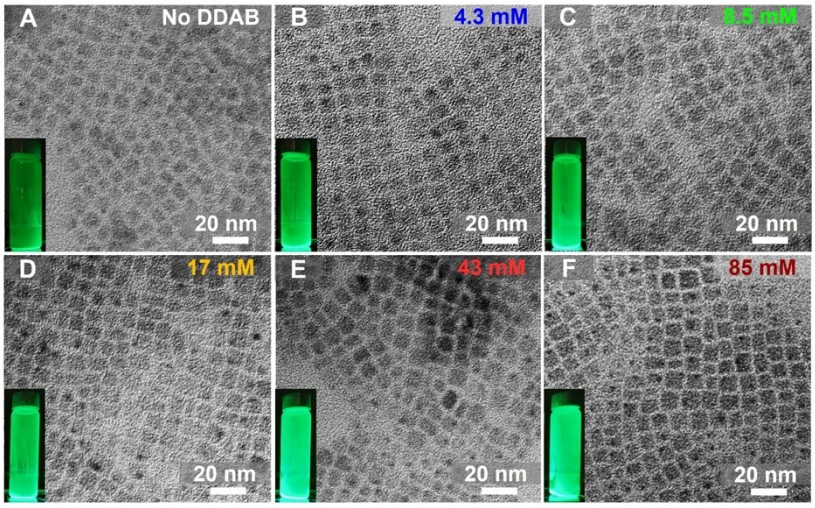

Figure S1. Typical TEM images of $CsPbBr_3$ PNCs dispersed into BuOH (A) in the absence of DDAB, and in the presence of (B) 4.3 mM, (C) 8.5 mM, (D) 17 mM, (E) 43 mM, and (F) 85 mM DDAB. Insets show the corresponding photographs of green luminescent PNCs dispersed in the DDAB/BuOH solutions.

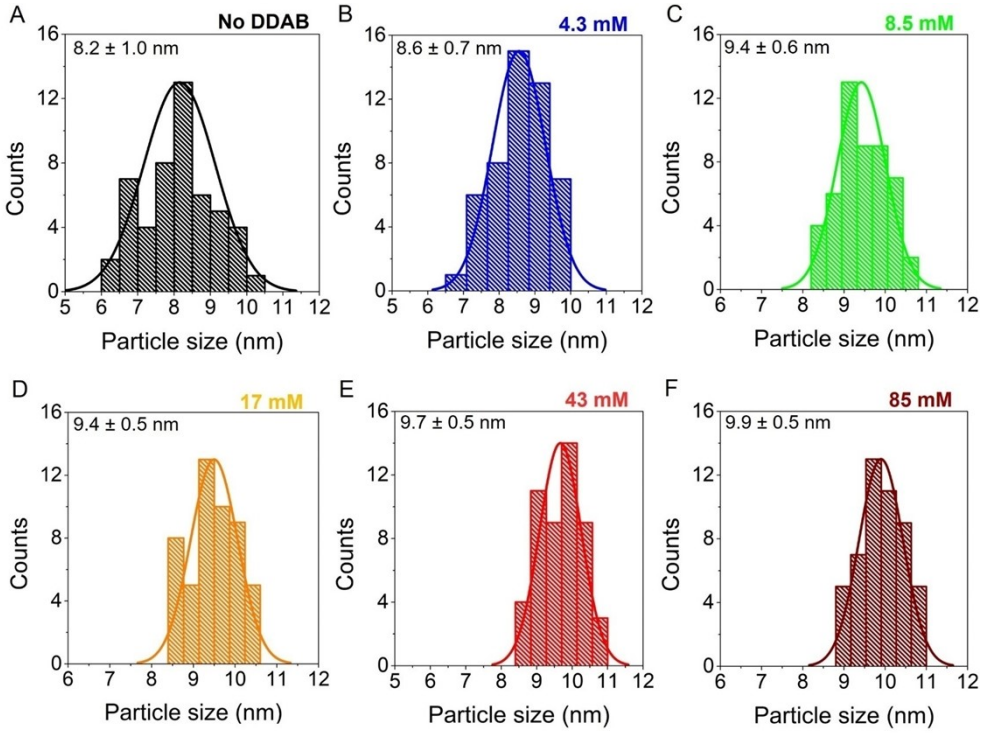

Figure S2. Histograms for estimating the particle size of $CsPbBr_3$ PNCs dispersed into BuOH (A) in the absence of DDAB, and in presence of (B) 4.3 mM, (C) 8.5 mM, (D) 17 mM, (E) 43 mM, and (F) 85 mM DDAB.

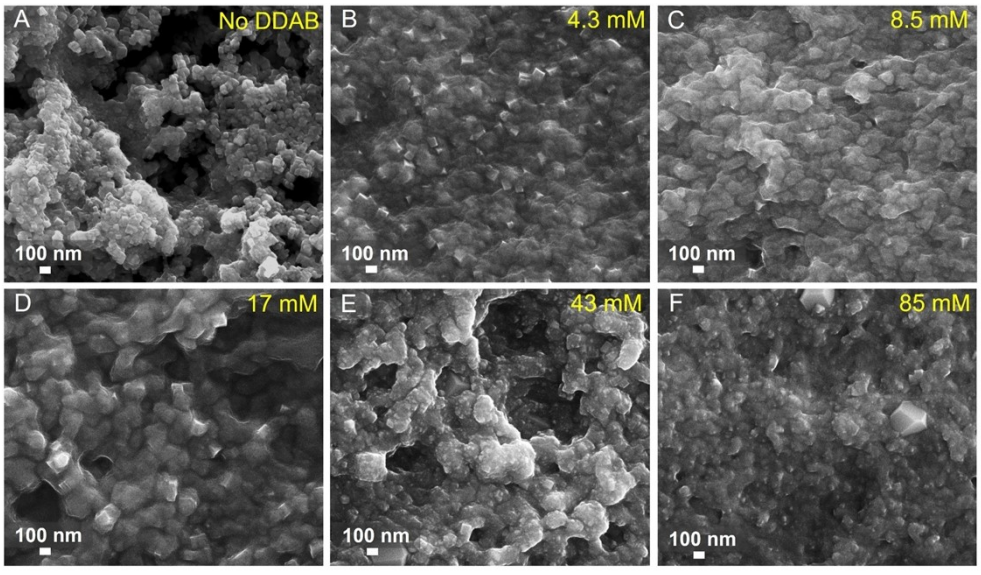

Figure S3. Top view SEM images of FTO/TiO_2/$CsPbBr_3$ PNCs photoanodes (A) in the absence and presence of different DDAB concentrations: (B) 4.3 mM, (C) 8.5 mM, (D) 17 mM, (E) 43 mM and (F) 85 mM.

Table S1. Average thickness of TiO_2 and PNCs layers from the as-prepared photoelectrodes obtained through cross-sectional SEM images.

Photoelectrode	Average TiO_2 layer thickness (µm)	Average PNCs layer Thickness (µm)
No DDAB	2.8 ± 0.1	0.5 ± 0.1
4.3 mM DDAB	3.1 ± 0.2	4.7 ± 0.2
8.5 mM DDAB	3.0 ± 0.1	6.8 ± 0.1
17 mM DDAB	2.7 ± 0.2	6.0 ± 0.3
45 mM DDAB	2.7 ± 0.2	2.9 ± 0.2
85 mM DDAB	2.9 ± 0.1	0.7 ± 0.1

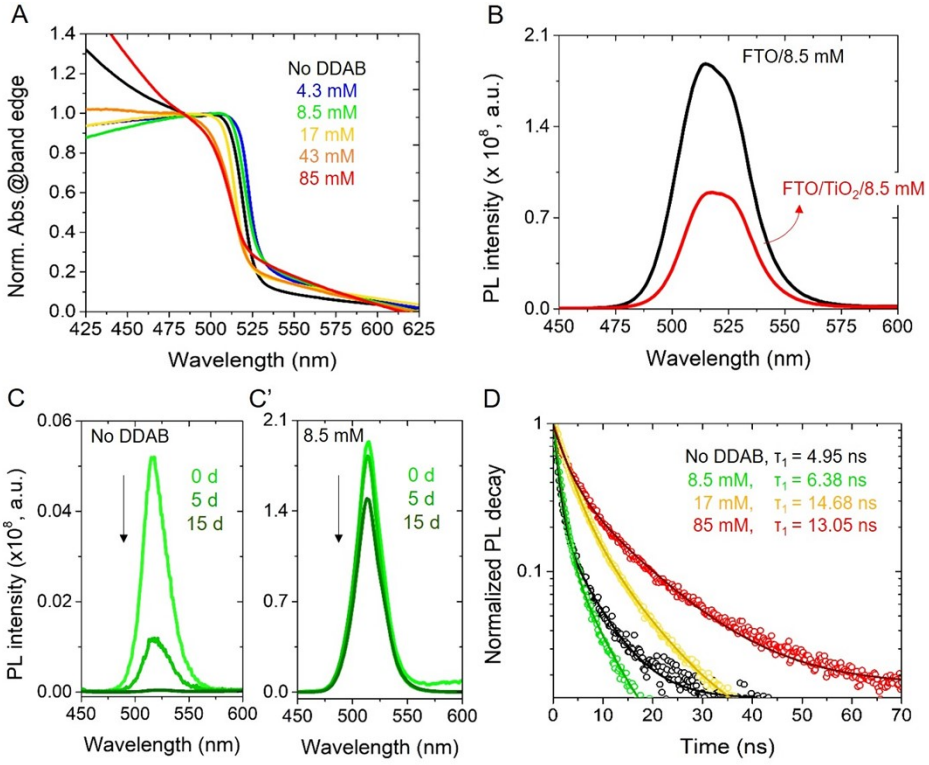

Figure S4. (A) UV-Vis spectra of $CsPbBr_3$ photoanodes in the presence and absence of different DDAB concentrations. (B) PL properties of the $CsPbBr_3$ photoanode in presence of 8.5 mM DDAB in presence (red curve) and absence (black curve) of m-TiO_2 layer. PL spectra of $CsPbBr_3$ photoanode (C) in the absence and (C') presence of 8.5 mM DDAB by varying the aging time under ambient conditions. (D) PL measurements of as-prepared $CsPbBr_3$ photoanodes by varying the DDAB concentration. PL decays were fitted using the bi-exponential equation $\tau_{avg} = A_1(\tau_1) + A_2(\tau_2)$, being τ_{avg}, the average PL lifetime, τ_1 and τ_2,

the PL decay time constants and A_1 and A_2, the relative amplitudes of the components, respectively. However, as τ_{avg} contains the longer component (τ_2) ascribed to re-absorption/re-emission of samples, we only used the faster decay component (τ_1) for characterizing the carrier recombination.

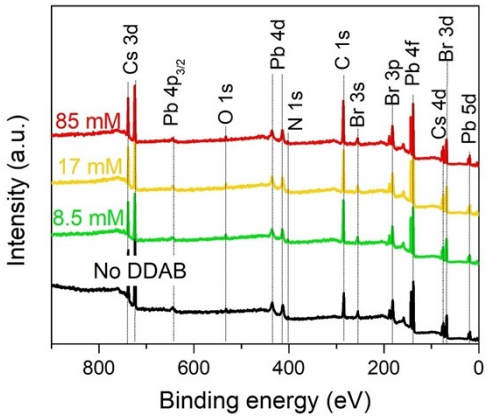

Figure S5. XPS survey spectra of $CsPbBr_3$ photoanodes with varying DDAB concentration.

Table S2. Chemical atomic composition of $CsPbBr_3$ photoanodes, in absence and presence of different DDAB concentrations, obtained by XPS.

Sample Identifier	Atomic Concentration (%)						Relative Concentrations					$O_{total}/(Br+O_{total})$
	C	O	Pb	Br	Cs	N	Cs	Pb	Br	N	O	
No DDAB	57.92	4.08	7.42	21.00	6.73	2.86	0.91	1.00	2.83	0.39	0.55	0.16
8.5 mM	73.46	3.11	4.35	12.06	4.50	2.52	1.03	1.00	2.77	0.58	0.71	0.20
17 mM	68.68	2.84	5.19	14.33	5.79	3.17	1.12	1.00	2.76	0.61	0.55	0.17
85 mM	70.73	2.44	4.75	13.48	5.42	3.18	1.14	1.00	2.84	0.67	0.51	0.15

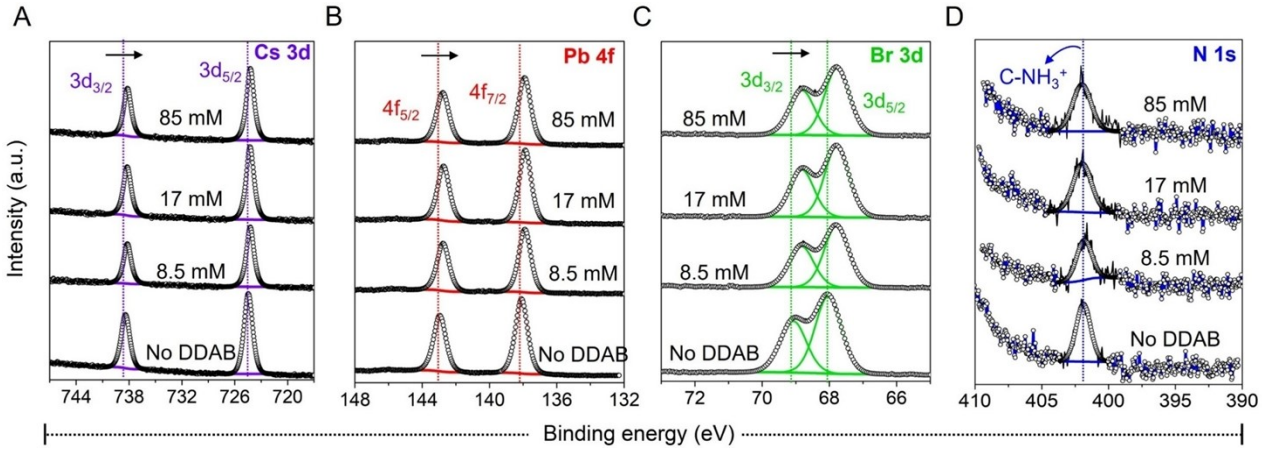

Figure S6. High-resolution XPS (A) Cs 3d, (B) Pb 4f, (C) Br 3d, and (D) N1s spectra of $CsPbBr_3$ photoanodes by varying DDAB concentration.

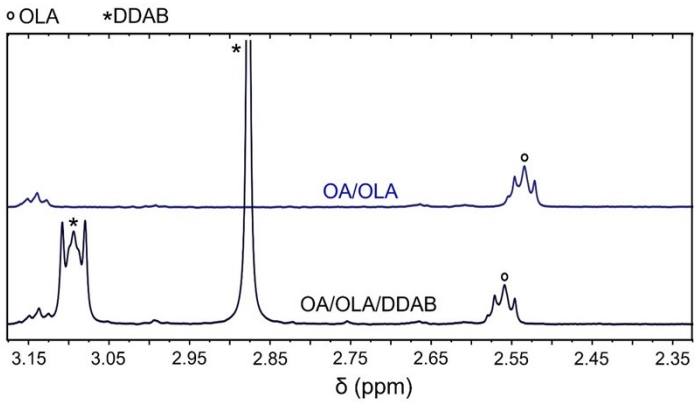

Figure S7. ^1H NMR (600 MHz, butanol-d_{10}/toluene-d_8 2:1 v/v, 298 K) spectra of OLA/OA/DDAB (black spectrum) and of OLA/OA (blue spectrum) mixtures, with expansion of the 3.20-2.30 ppm spectral region.

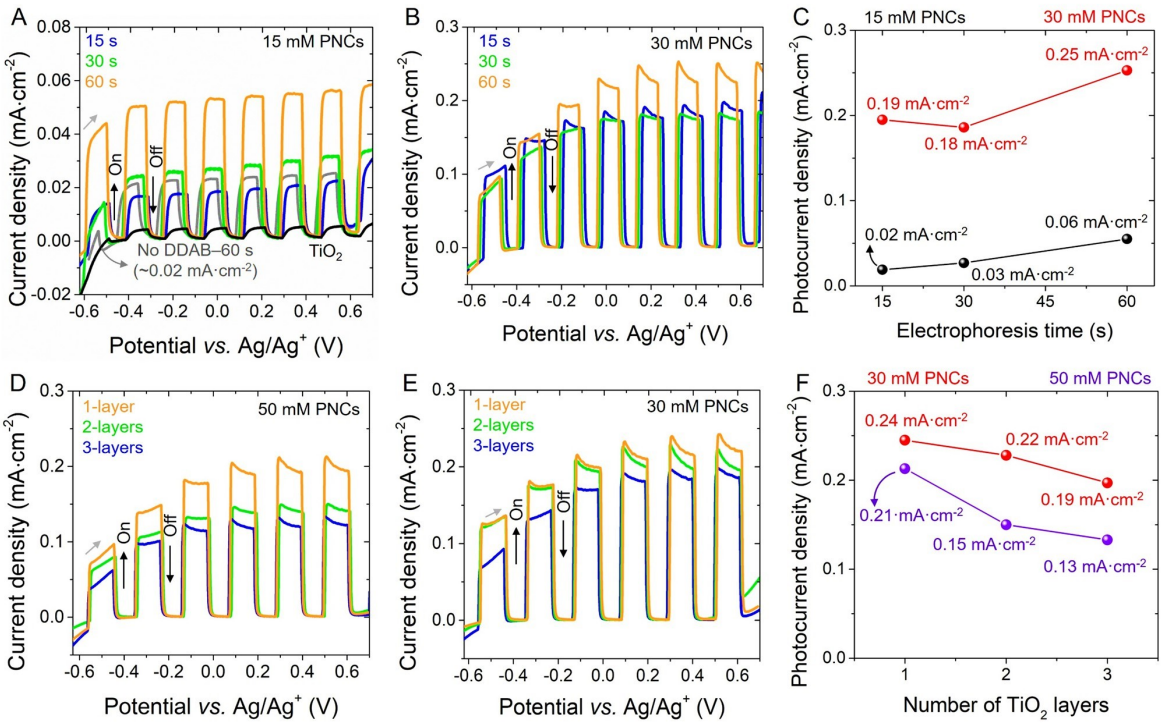

Figure S8. Chopped light voltammetry measurements showing the photocurrents of TiO_2 and $CsPbBr_3$ photoanodes in the absence and presence of 85 mM DDAB under visible illumination (100 mW·cm^{-2}, UV filter) in 45 mM MeBr/BuOH electrolyte. The measurements were performed by varying main fabrication parameters: PNCs concentration for ED process: (A) 15 mM, (B, E) 30 mM, and (D) 50 mM (60 s deposition), employing different deposition times in (A) and (B), and studying the effect of the number of TiO_2 layers on the PEC activity of photoanodes in (D) and (E). Maximum photocurrent generated by the photoanodes as a function of (C) ED time and (F) number of TiO_2 layers.

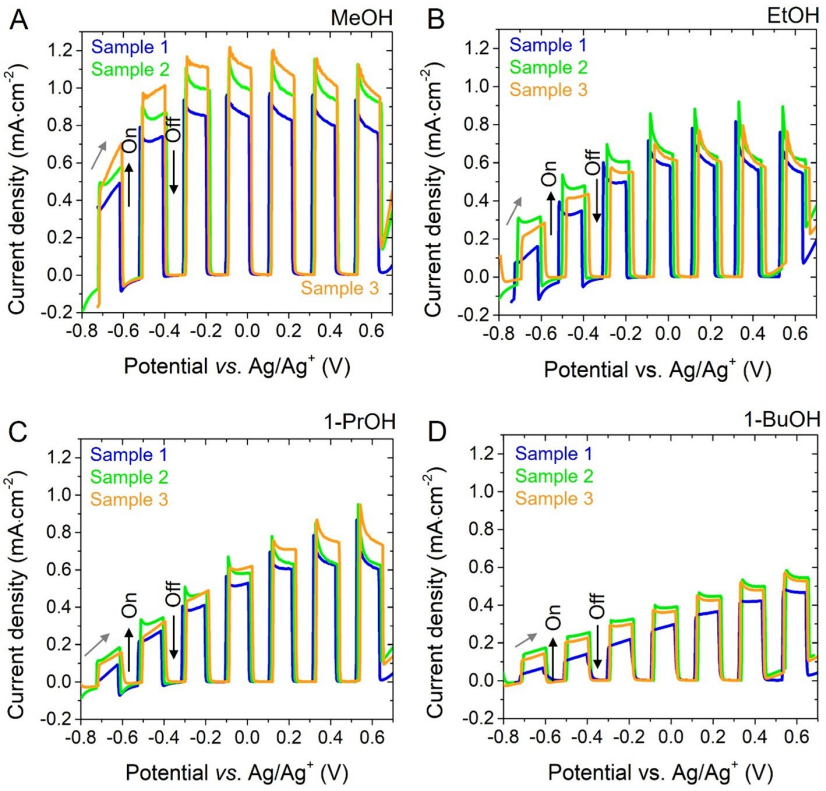

Figure S9. Chopped light voltammetry measurements showing the photocurrents of $CsPbBr_3$ photoanodes in presence of 8.5 mM DDAB under visible illumination (100 mW·cm^{-2}, UV filter) in 45 mM MeBr in different alcohol electrolytes: (A) MeOH, (B) EtOH, (C) 1-PrOH and (D) 1-BuOH. Three different samples were studied for reproducibility in each alcohol environment.

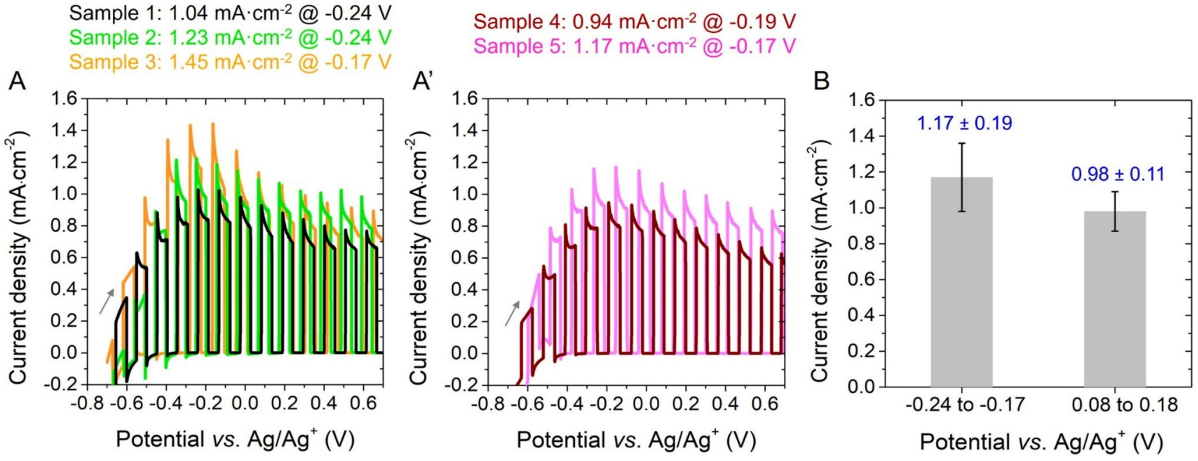

Figure S10. (A, A') Reproducibility in the PEC activity of five $CsPbBr_3$ photoanodes in presence of 8.5 mM DDAB under visible illumination (100 mW·cm^{-2}, UV filter) in 45 mM MeBr/MeOH electrolyte, showing the maximum photocurrent generated by each photoactive material. (B) average photocurrent (with

error bars from five diverse samples) at two potential ranges: from -0.24 to -0.17 V *vs*. Ag/Ag^+ and from 0.08 to 0.18 V *vs*. Ag/Ag^+.

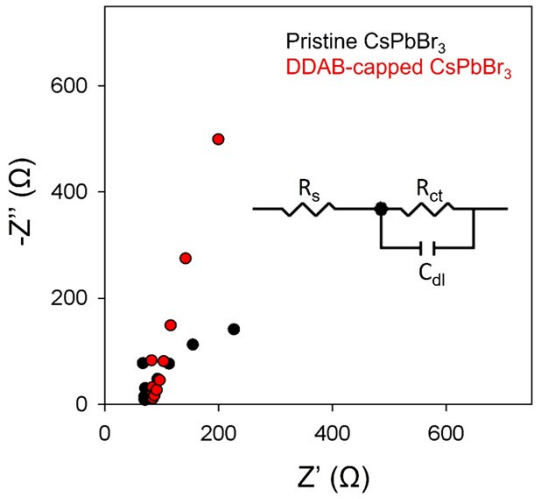

Figure S11. Nyquist plots obtained for $CsPbBr_3$ photoanodes in absence (black dot) and presence of DDAB ligand (red dot) under visible illumination (100 $mW \cdot cm^{-2}$, UV filter) in 45 mM MeBr/MeOH electrolyte, by applying a bias of 0.1 V *vs*. Ag/Ag^+ in a frequency range of 100 kHz – 0.1 Hz. A Randles-type equivalent circuit model was employed for the fitting of EIS curves.

Table S3. Extracted parameters of fitted EIS curves: Series resistance (R_s), Interfacial carrier transport resistance (R_{ct}) and double-layer capacitance (C_{dl}).

Photoanode	**R_s (Ω)**	**R_{ct} (Ω)**	**C_{dl} (F)**
Pristine $CsPbBr_3$	75.68	239.6	2.86×10^{-5}
DDAB-capped $CsPbBr_3$	89.19	1970	1.68×10^{-5}

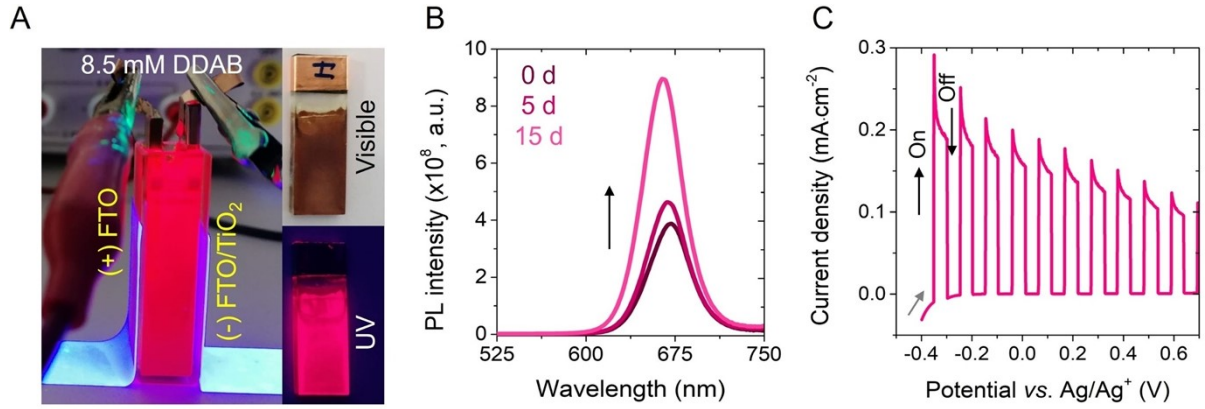

Figure S12. (A) Electrophoretic deposition of red-emitting $CsPbI_3$ PNCs on an FTO/TiO_2 electrode in the presence of 8.5 mM DDAB in BuOH solution, at 250 V for 60 s. (B) PL spectra of $CsPbI_3$ photoanode by varying aging times under ambient conditions. (C) Chopped light voltammetry measurements showing the photocurrent of $CsPbI_3$ photoanodes in the presence of 8.5 mM DDAB under visible illumination (100 mW·cm^{-2}, UV filter) in 45 mM MeBr/MeOH electrolyte.

Determination of Faradaic efficiency for CH_2O formation

From chronoamperometry profile obtained during PEC MeOH oxidation using the $CsPbBr_3$ photoanode in presence of 8.5 mM, see **Figure 4B**, it was possible to calculate a Q = 0.181 C. In this context, using Faraday´s Law described above, $\eta_{theoretical} = 9.38\ x\ 10^{-7}\ mol$ and therefore, $[\,]_{theoretical} = 3.75\ x10^{-5}\ M$ (in 25 mL of electrolyte solution). Converting this value in ppm by multiplying the Molar concentration with CH_2O molar weight $(30.03\ x\ 10^3 mg)$, a concentration of 1.12 ppm is estimated. Later, by obtaining three different aliquots from the electrolyte solution [at t = 0 (blank under dark), and t = 1800 s under visible light in absence (photolysis) and presence of photoanode], we proceed to estimate the experimental concentration of CH_2O in these samples by using UV-Vis spectroscopy. As seen in **Figure S13A**, five CH_2O pattern solutions were prepared (0, 0.5, 1.0, 2.0 and 4.0 ppm), which were required to obtain their corresponding absorbance using a calibration curve with a Pearson´s r = 0.99974, see **Figure S13B**. The blank and the sample obtained after photolytic reaction exhibit a low fraction of formed CH_2O, indicating that some MeOH exhibit initially some partial oxidation to produce CH_2O (0.09 ppm CH_2O), possibly caused by its interaction with oxygen from ambient air. Then, after PEC oxidation, it was estimated the formation of 0.76 ppm CH_2O. Accordingly, the net CH_2O concentration produced during MeOH oxidation was 0.76 ppm – 0.09 ppm = 0.67 ppm CH_2O. Thus:

$$FE\ (\%) = \frac{[\,]_{experimental}}{[\,]_{theoretical}} x\ 100; FE = \frac{0.67\ ppm\ CH_2O}{1.12\ ppm\ CH_2O}\ x\ 100; FE = 59.8\%$$

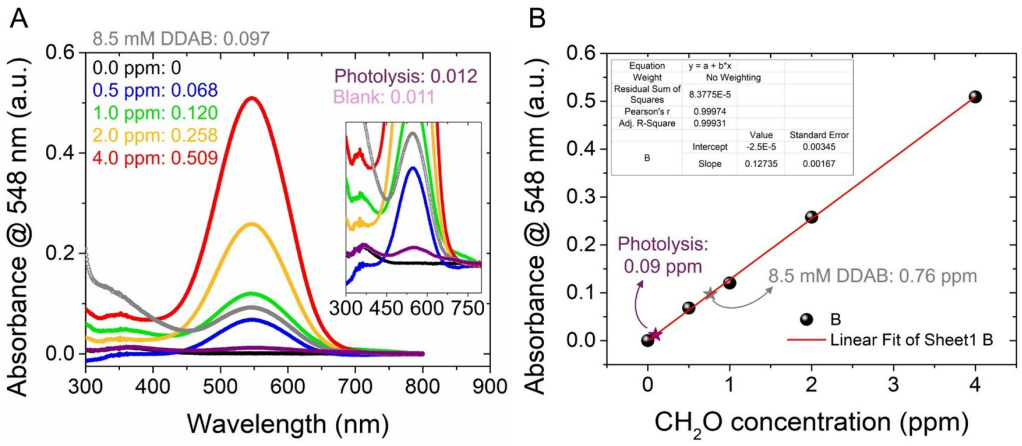

Figure S13. (A) UV-Vis spectra and (B) the corresponding calibration curve of CH_2O pattern solutions to carry out the quantitative determination of CH_2O concentration from samples extracted from the electrolyte solution at t=0 under dark (blank), and after 1800 s under visible light illumination (100 $mW \cdot cm^{-2}$, UV filter) in absence (photolysis) and presence of $CsPbBr_3$ photoanode modified with 8.5 mM DDAB at 0.1 V *vs*. Ag/Ag^+. Inset shows the UV-Vis spectra of blank and sample after photolytic reaction.

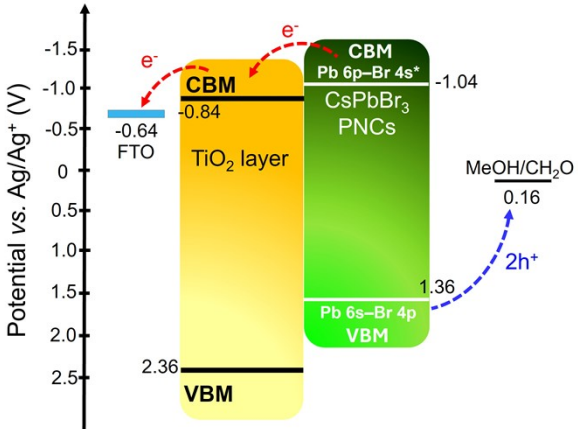

Figure S14. Band diagram of the $FTO/TiO_2/CsPbBr_3$ photoanode and redox potential of $MeOH/CH_2O$ system extracted from the literature.[2, 3] Values were converted into Ag/Ag^+ reference (Ag/Ag^+ = 0.54 V *vs*. NHE).

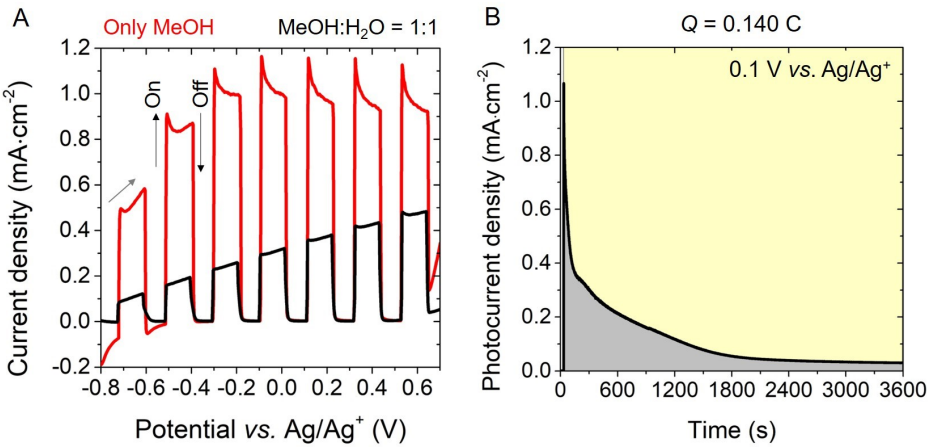

Figure S15. (A) Chopped-light voltammetry showing the photocurrent from $CsPbBr_3$ photoanodes in the presence of 8.5 mM DDAB in full MeOH environment (red curve) and a polar solvent mixture based on MeOH:H_2O volume ratio = 1:1 (black curve). (B) Chronoamperometry profile of a $CsPbBr_3$ photoanode in the presence of 8.5 mM DDAB during photoelectrolysis by applying a bias of 0.1 V *vs*. Ag/Ag^+ for 3600 s in MeOH. Experimental conditions: visible illumination (100 $mW \cdot cm^{-2}$, UV filter), electrolyte: 45 mM MeBr.

References

(1) Jacobsen, N. W.; Dickinson, R. G. Spectrometric assay of aldehydes as 6-mercapto-3-substituted-s-trizolo(4,3-b)-tetrazines. *Analytical Chemistry* **2002**, *46* (2), 298-299. DOI: 10.1021/ac60338a039.

(2) Fernández-Climent, R.; Gualdrón-Reyes, A. F.; García-Tecedor, M.; Mesa, C. A.; Cárdenas-Morcoso, D.; Montañes, L.; Barea, E. M.; Mas-Marzá, E.; Julián-López, B.; Mora-Seró, I.; et al. Switchable All Inorganic Halide Perovskite Nanocrystalline Photoelectrodes for Solar-Driven Organic Transformations. *Solar RRL* **2021**, *6*, 2100723. DOI: 10.1002/solr.202100723.

(3) Korzeniewski, C.; Childers, C. L. Formaldehyde Yields from Methanol Electrochemical Oxidation on Platinum. *The Journal of Physical Chemistry B* **1998**, *102* (3), 489-492. DOI: 10.1021/jp9731157.